Model Catalytic Studies of Liquid Organic Hydrogen Carriers: Dehydrogenation and Decomposition Mechanisms of Dodecahydro-N-ethylcarbazole on Pt(111)

Max Amende,[†] Christoph Gleichweit,[†] Kristin Werner,[†] Stefan Schernich,[†] Wei Zhao,[†] Michael P. A. Lorenz,[†] Oliver Höfert,[†] Christian Papp,[†] Marcus Koch,[‡] Peter Wasserscheid,[‡,§] Mathias Laurin,[†] Hans-Peter Steinrück,[†,§] and Jörg Libuda*[,†,§]

[†]Lehrstuhl für Physikalische Chemie II, [‡]Lehrstuhl für Chemische Reaktionstechnik, and [§]Erlangen Catalysis Resource Center, Friedrich-Alexander-Universität Erlangen-Nürnberg, Egerlandstrasse 3, 91058 Erlangen, Germany

S *Supporting Information*

ABSTRACT: Liquid organic hydrogen carriers (LOHC) are compounds that enable chemical energy storage through reversible hydrogenation. They are considered a promising technology to decouple energy production and consumption by combining high-energy densities with easy handling. A prominent LOHC is N-ethylcarbazole (NEC), which is reversibly hydrogenated to dodecahydro-N-ethylcarbazole (H_{12}-NEC). We studied the reaction of H_{12}-NEC on Pt(111) under ultrahigh vacuum (UHV) conditions by applying infrared reflection−absorption spectroscopy, synchrotron radiation-based high resolution X-ray photoelectron spectroscopy, and temperature-programmed molecular beam methods. We show that molecular adsorption of H_{12}-NEC on Pt(111) occurs at temperatures between 173 and 223 K, followed by initial C−H bond activation in direct proximity to the N atom. As the first stable dehydrogenation product, we identify octahydro-N-ethylcarbazole (H_8-NEC). Dehydrogenation to H_8-NEC occurs slowly between 223 and 273 K and much faster above 273 K. Stepwise dehydrogenation to NEC proceeds while heating to 380 K. An undesired side reaction, C−N bond scission, was observed above 390 K. H_8-NEC and H_8-carbazole are the dominant products desorbing from the surface. Desorption occurs at higher temperatures than H_8-NEC formation. We show that desorption and dehydrogenation activity are directly linked to the number of adsorption sites being blocked by reaction intermediates.

KEYWORDS: infrared spectroscopy, photoelectron spectroscopy, molecular beams, mass spectrometry, liquid organic hydrogen carrier, model catalysis
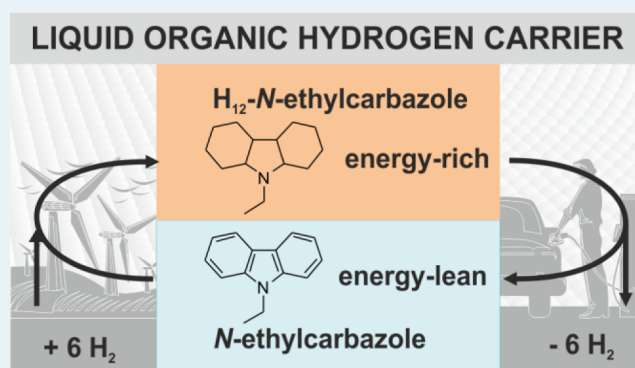
INTRODUCTION

The transition to renewable sources of energy is linked to the problem that the availability of sun and wind energy is highly intermittent and depends on meteorological factors that are hard to control. Thus, for a high share of renewable energy in electricity production, sun and wind energy "overproduction" at "energy-rich" times (sun is shining, wind is blowing) must be efficiently stored for utilization at "energy-lean" times (night, no wind is blowing). Among the compounds for chemical energy storage, hydrogen is by far the most efficient from a gravimetric point of view;[1] however, the drawbacks of physical storage methods, that is, liquid or compressed,[1−5] are apparent. To avoid cryogenic temperatures or high pressures, new hydrogen storage technologies are required that are cost-efficient, safe, and easily applicable at larger scale. These requirements are met by the concept of so-called "liquid organic hydrogen carriers" (LOHCs).[6−10] The idea is based on the catalytic conversion of energy-lean to energy-rich organic compounds through reversible hydrogenation and dehydrogenation. Once loaded with hydrogen (produced, e.g., via water electrolysis at energy-rich times), these carriers can be easily transported and stored without any loss, making use of the existing transport and storage logistics of liquid fuels. At the desired place and energy-lean times, hydrogen is released, for example, for combustion or to operate a fuel cell. The dehydrogenated, energy-lean compound is again rehydrogenated at energy-rich times without being consumed (note that hydrogenation and dehydrogenation are separate processes, typically performed under different conditions and on different catalysts). Recently, the potential of LOHC technology has been analyzed in detail, for both mobile[7] and stationary[8] applications.

Finding the ideal LOHC system is not trivial. A suitable LOHC pair should combine the appropriate physical and chemical properties (e.g., suitable melting points, favorable hydrogenation thermodynamics, high thermal stability), it should have low toxicity, and it must be easily available at a large scale and at a low price, with a low level of impurities that may be harmful for the hydrogenation/dehydrogenation catalyst.[7] Among the potential carrier molecules, heterocyclic aromatic hydrocarbons are promising candidates.[11−13] Particularly, N-ethylcarbazole (NEC) has been identified as a high-potential contender for an energy-lean LOHC compound (see Figure 1a).[14] Through reversible hydrogenation to dodecahy-

Figure 1. (a) Reaction scheme of hydrogenation and dehydrogenation of NEC and H$_{12}$-NEC, respectively. (b) IR spectra recorded during H$_{12}$-NEC exposure of Pt(111) under isothermal conditions at selected temperatures. The spectra were recorded after 30 min of exposure.

dro-N-ethylcarbazole (H$_{12}$-NEC), NEC is capable to store 5.8 wt % H$_2$.[7] Although this value is attractive, challenges remain in the field of catalyst development, for example, the minimization (or even elimination) of the noble metal content, maximization of reaction rates at low temperatures, and the optimization of selectivity to avoid undesired side reactions.

Understanding the dehydrogenation mechanisms is therefore critical toward the development of better catalysts; however, not much is known about the detailed reaction mechanisms of

LOHCs such as H$_{12}$-NEC at the microscopic scale. Molecular insights into the catalytic reaction mechanisms and the associated microkinetics can be obtained from model studies using a surface science approach.[15−17]

Previously, we showed that H$_{12}$-NEC adsorbs molecularly on Pd(111)[18] and supported Pd nanoparticles[19] at cryogenic temperatures. Initial C−H bond activation at the α-carbons takes place at about 170 K on the nanoparticles and 200 K on the planar surface. Such an activation is in line with the theoretical work by Sotoodeh and Smith,[20] stating that H$_8$-NEC is the first stable reaction intermediate. H$_8$-NEC starts to desorb from the Pd(111) surface at 330 K, and the maximum reaction rate is reached at 550 K. An important finding is the abstraction of the ethyl side chain at elevated temperature and subsequent decomposition to small molecular fragments, finally yielding atomic carbon and nitrogen. This reaction pathway is similar to other hydrocarbons on transition metal surfaces at elevated temperature.[21,22] Note that C−N bond scission is found both on real catalysts and in surface science studies, but the rate is much higher in the latter case, that is, on clean surfaces and at low pressure.

Here, we present the results of such a surface science study on Pt(111), combining temperature-programmed, high-resolution X-ray photoelectron spectroscopy (HRXPS), temperature-programmed molecular beam (TPMB) experiments, and infrared absorption−reflection spectroscopy (IRAS), analyzing both surface species and gas phase products. This study follows a short communication in which the adsorption of H$_{12}$-NEC on Pt(111) at 140 K and the subsequent thermal evolution were studied solely by HRXPS.[23] In contrast to the latter work, we explore the reaction during continuous supply of the reactant. This temperature-programmed reaction study using HRXPS and TPMB provides data on both the surface species and the desorbing products, thus enabling insight into the influence of adsorbates on the dehydrogenation mechanism. In addition, the presented data on Pt(111) allow for a comparison with our recent study on Pd(111).[18] We also introduce an improved TPMB measurement procedure to identify reaction products in the gas phase.

RESULTS AND DISCUSSION

Interaction of H$_{12}$-NEC with Pt(111) Studied by IRAS. In the first step, the interaction of H$_{12}$-NEC with the clean Pt(111) surface was studied by IRAS under isothermal conditions. H$_{12}$-NEC was deposited by physical vapor deposition (PVD) at several temperatures ranging from 100 to 473 K. The deposition process was continuously followed by IR spectroscopy in time-resolved (TR) mode. Representative spectra for each temperature are displayed in Figure 1b. The complete series of time-resolved spectra are provided in Figure S1 in the Supporting Information.

The most prominent features in the low temperature region (100 to 173 K) are CH$_2$ deformation bands around 1450 cm^{-1}, the CH stretching vibration at 2791 cm^{-1}, the CH$_2$ symmetric stretching modes at 2851 cm^{-1}, the CH$_2$ asymmetric stretching modes at 2930 cm^{-1}, and the CH$_3$ asymmetric stretch modes at 2963 cm^{-1}. The assignment of the bands is based on DFT calculations and was discussed in more detail in our previous publications.[18,19]

Comparison of these spectra with those of the multilayer of H$_{12}$-NEC physisorbed on Pd(111)[18] at 100, 123, and 173 K does not reveal any difference, indicating that at temperatures up to 173 K, multilayers of H$_{12}$-NEC adsorb molecularly on
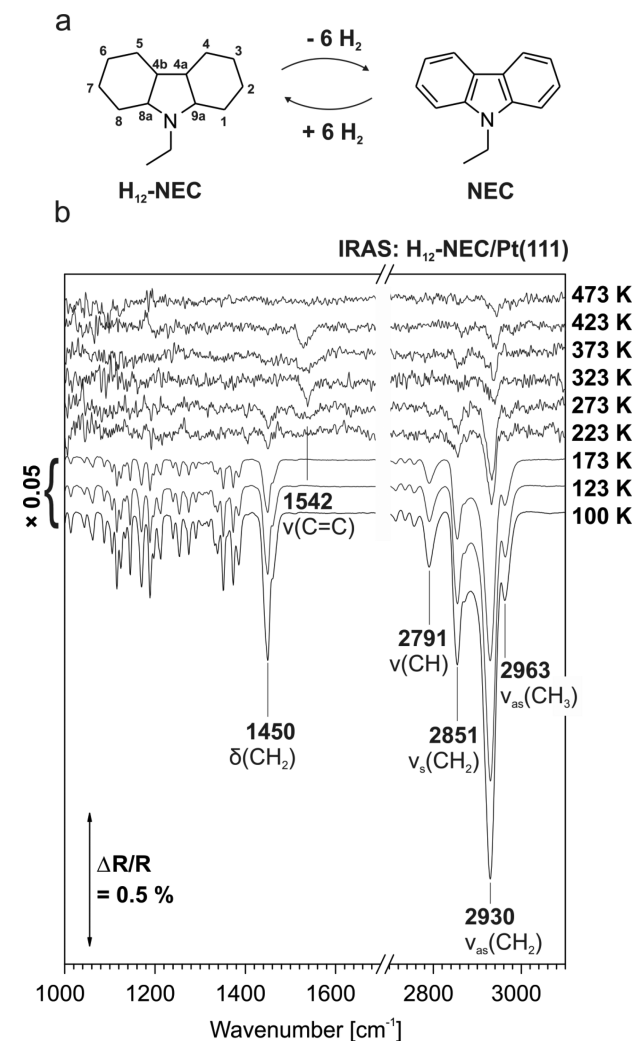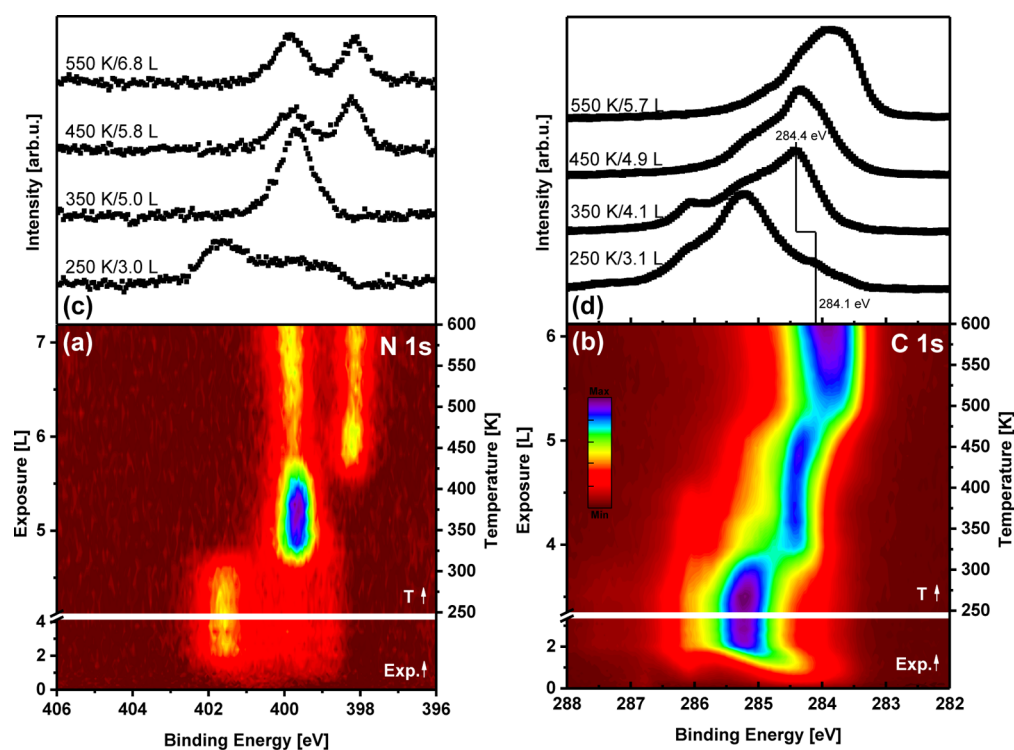
Figure 2. XP spectra of the ramping experiment of H_{12}-NEC on Pt(111). (a) N 1s spectra and (b) C 1s spectra of the adsorption and reaction as a color-coded density plot. (c, d) Selected spectra of the experiments.

Pt(111) without decomposition. We underline that this holds true even at 173 K, in contrast with our previous H_{12}-NEC adsorption experiments on a Pd/Al$_2$O$_3$/NiAl(110) model system, in which first evidence of dehydrogenation (new band at 1547 cm^{-1}) was observed already at this temperature.[19] On Pt(111), no multilayer is formed at 223 K and above, which is deduced from the significant decrease in intensity of all bands at large exposures. On the basis of the fact that neither new bands are observed nor any significant change in relative intensity is found up to 173 K, we exclude conversion of the fully hydrogenated LOHC compound on Pt(111) up to this temperature. By comparing the time-resolved adsorption spectra (see Figure S1 of the Supporting Information) at 223 K with those at lower temperatures, differences are revealed. Multilayer formation up to 173 K is reflected by a constant increase in all bands over the entire exposure time, whereas at 223 K, saturation after a 2 min exposure indicates formation of a monolayer. At 273 K, a shallow band becomes visible at 1542 cm^{-1} (Supporting Information Figure S1). A similar band was also observed in the H_{12}-NEC/Pd(111) system. On the basis of DFT calculations, it was attributed to the C=C vibrational modes of a partially dehydrogenated intermediate with a fully aromatic five-membered ring, that is, with the hydrogen atoms being abstracted from the positions 4a, 4b, 8a, and 9a. This intermediate is hereafter referred to as H_8-NEC. Considering the CH$_2$ and CH vibrational modes, no significant differences are observed between 223 and 273 K.

We should point out here for further discussion that the band at 2791 cm^{-1} is exclusively localized at the α-carbon atoms in the carbazole skeleton (positions 8a and 9a). According to our previous findings, the initial step of dehydrogenation is manifested in cleavage of the C−H bonds at these positions. This process is generally reflected by a decrease or disappearance of the CH vibration at 2791 cm^{-1} but can

hardly be followed by IRAS because of the low intensity of this band.

At 323 K, we clearly observe a decrease in intensity of the CH$_2$ stretching signal, whereas the CH$_2$ deformation at 1450 cm^{-1} and the CH vibration at 2791 cm^{-1} completely vanish. At the same time, the band at 1542 cm^{-1} that we associated with H_8-NEC grows considerably. It remains visible up to temperatures of 423 K. The low intensity of this band at 273 K indicates only partial conversion of H_{12}-NEC to H_8-NEC up to this temperature, whereas at 323 K, the H_8-NEC species dominates (indicated by both the increase in the band at 1542 cm^{-1} and the disappearance of the CH vibrational mode). This observation matches our HRXPS results discussed below.

It is noteworthy that the CH$_2$ stretching vibrations are weakened in intensity and the CH$_3$ stretching vibrations completely disappear above 273 K. In contrast with the experiments on Pd(111), weak signals are observed in the high-frequency region up to the highest temperatures investigated. On Pd(111), practically no IR bands are observed above 323 K. However, the decreasing IR band intensities upon heating cannot necessarily be associated with desorption, since H_{12}-NEC fragments with very low IR activity may be formed on the surface. Especially planar intermediates oriented parallel on the surface lead to very low IR activity of most bands as a result of the metal surface selection rule (MSSR).[24,25] Computational studies by Sotoodeh and Smith on H_8-NEC on Pd(111) show that the pyrrole unit is oriented almost parallel to the metal surface.[20] Since the surface coverage in our experiments above 273 K might be too high to allow the favored flat orientation of H_8-NEC on Pt(111),[26] the C=C stretching mode at 1542 cm^{-1} becomes clearly visible at 323 K. In a flat-lying orientation, the band would be very weak as a result of the MSSR and due to the modified surface bonding with partial π and σ character.[27−31] The HRXPS experiments discussed below

indeed verify the presence of dehydrogenation and decomposition products in all temperature regimes.

Interestingly, we observe a decrease in the CH_2 and CH_3 vibrational modes when heating from 273 to 473 K. As stated above, the molecule dehydrogenates to H_8-NEC between 273 and 323 K. Because C−H bond activation and dehydrogenation to H_8-NEC is not expected to affect CH_2 or CH_3 vibrations in a direct manner, we may speculate that weakening of the bands at 2791, 2851, 2930, and 2963 cm^{-1} may also result from a change in adsorption geometry. Finally, we note that both HRXPS and TPMB analyses indicate further reactions at higher temperature, namely, dehydrogenation of the six-membered rings and C−N bond cleavage. Neither transformation could be directly traced by IRAS, yet they may contribute to the weakening of CH_2 and CH_3 bands above 273 K.

Reaction Mechanisms of H_{12}-NEC on Pt(111) Studied by HRXPS. Synchrotron radiation-based HRXPS allows us to follow the reaction steps on the surface in great detail. This is done by analyzing chemical shifts that reflect the chemical bonding and environment of the atoms. The experiments were performed by first adsorbing H_{12}-NEC on a clean Pt(111) surface at 250 K until saturation was reached. Adsorption at this temperature prevents multilayer formation (as IR shows in the previous section). Subsequently, a heating ramp of 0.5 K s^{-1} was applied while the crystal was exposed to H_{12}-NEC at a constant background pressure of ∼8 × 10^{-9} mbar. This procedure constantly supplies fully loaded LOHC molecules while heating and thereby mimics the conditions of the TPMB experiment (see below). Because H_{12}-NEC dehydrogenation on real catalysts is performed around 500 K, we restrict ourselves to temperatures below 600 K. Spectra were measured continuously, providing complementary information to the IRAS and TPR experiments. Note that in our previous study,[23] a multilayer was adsorbed, and the heating ramp was applied without continuous dosing.

For the C 1s and N 1s core levels, separate experiments under the same conditions were performed. The complete data sets are shown in Figure 2a and b in a color-coded density plot. Note that there is an exposure and a temperature scale, since the sample is exposed to the molecule in the gas phase even during heating. Selected spectra, representative for the different species appearing throughout the temperature ramp, are shown in Figure 2c and d. In addition, the quantitative analysis of the N 1s (Figure 2a) and C 1s (Figure 2b) spectra as a function of exposure is shown in Figure 3.

During the first part of the experiments, H_{12}-NEC is dosed at constant temperature until saturation of the monolayer. Initially, peaks at 401.6 eV in the N 1s and at 284.1 eV in the C 1s region develop. Up to an exposure of ∼2 L (Langmuir; 1 L = 1.33 × 10^{-6} mbar·s), the C 1s peak shifts toward higher binding energies (285.2 eV) while a shoulder at 284.1 eV remains. In the N 1s region, another signal appears at 399.8 eV. From previous work,[23] the signals at 401.6 eV in the N 1s region and 285.2 eV in the C 1s region are attributed to the H_{12}-NEC monolayer. The additional N 1s peak at 399.8 eV is assigned to the partially dehydrogenated product H_8-NEC. Therefore, we suggest that the molecule partially dehydrogenates at low coverage, whereas dehydrogenation is suppressed at saturation as a result of space limitations. The latter may arise from adsorbed hydrogen that may block reaction sites. Conversion to H_8-NEC mainly changes the surroundings of the α-carbon atoms of the pyrrole ring and, hence, can be observed in the N 1s region.
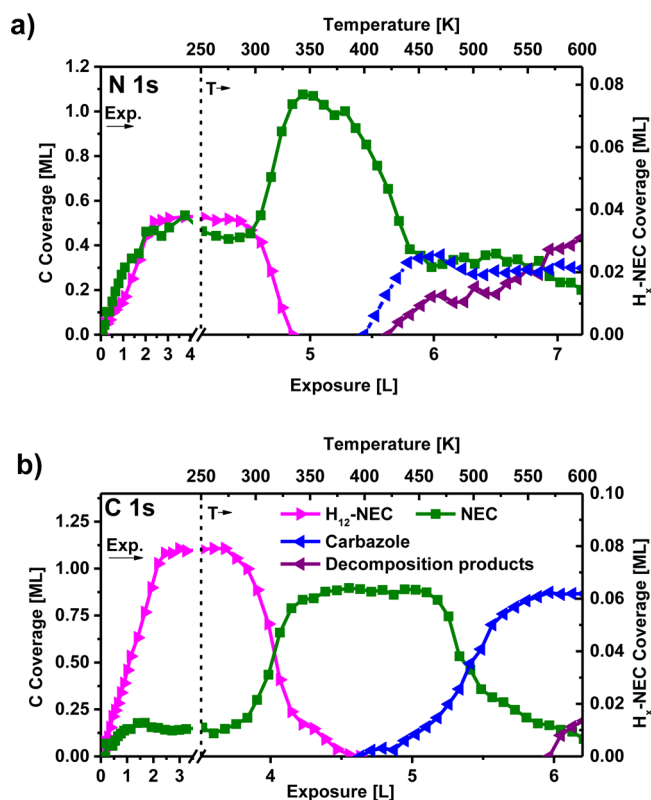

Figure 3. Quantitative analysis of the XPS experiments with H_{12}-NEC shown in Figure 2. (a) Analysis of the N 1s spectra of the adsorption and reaction; (b) the respective analysis of the C 1s region. The dashed lines indicate the start of the heating ramp. Note that the H_{12}-NEC signal and also the NEC signal contain contributions from H_x-NEC (for details, see text).

The quantitative analysis of the nitrogen peak areas (see Figure 3a) shows that, at saturation, ∼40% of H_8-NEC coexists with 60% of H_{12}-NEC. This situation is also reflected in the C 1s region. For the quantitative analysis of the C 1s spectra shown in Figure 3b, we used envelopes consisting of two Doniach−Sunjic functions each, for H_{12}-NEC (main line at 285.2 eV) and NEC (main line at 284.1 eV).[23] These two peaks are an envelope of the large variety of carbon atoms in different chemical surroundings in the molecule and carbon atoms in different adsorption positions on the surface and should not be mistaken as two distinct chemical species. This assignment to only two different chemical species cannot account for the stepwise dehydrogenation. However, if (in a simplified picture) we consider the peak at 285.2 eV as arising mainly from saturated carbon atoms of H_X-NEC (CH_2/CH in the benzene/pyrrole ring) and the peak at 284.1 eV due to unsaturated carbon atoms of H_X-NEC (CH/C in the benzene/pyrrole ring), we should be able to explain the observed behavior. Indeed, by attributing the peak at 284.1 eV to the four dehydrogenated pyrrole carbon atoms in H_8-NEC, the corresponding C 1s signal for complete conversion to H_8-NEC should be 29% (4 out of 14 carbon atoms) of the total signal. The observed intensity of 13% in Figure 3b thus indicates a conversion of 45%, which is in close agreement to the value of 40% derived from the N 1s spectra.

Next, we address the thermal evolution of the adsorbed species. In the N 1s region, the peak of the fully hydrogenated H_{12}-NEC decreases at 280 K and vanishes completely at 340 K. This corresponds to full dehydrogenation of the pyrrole ring,
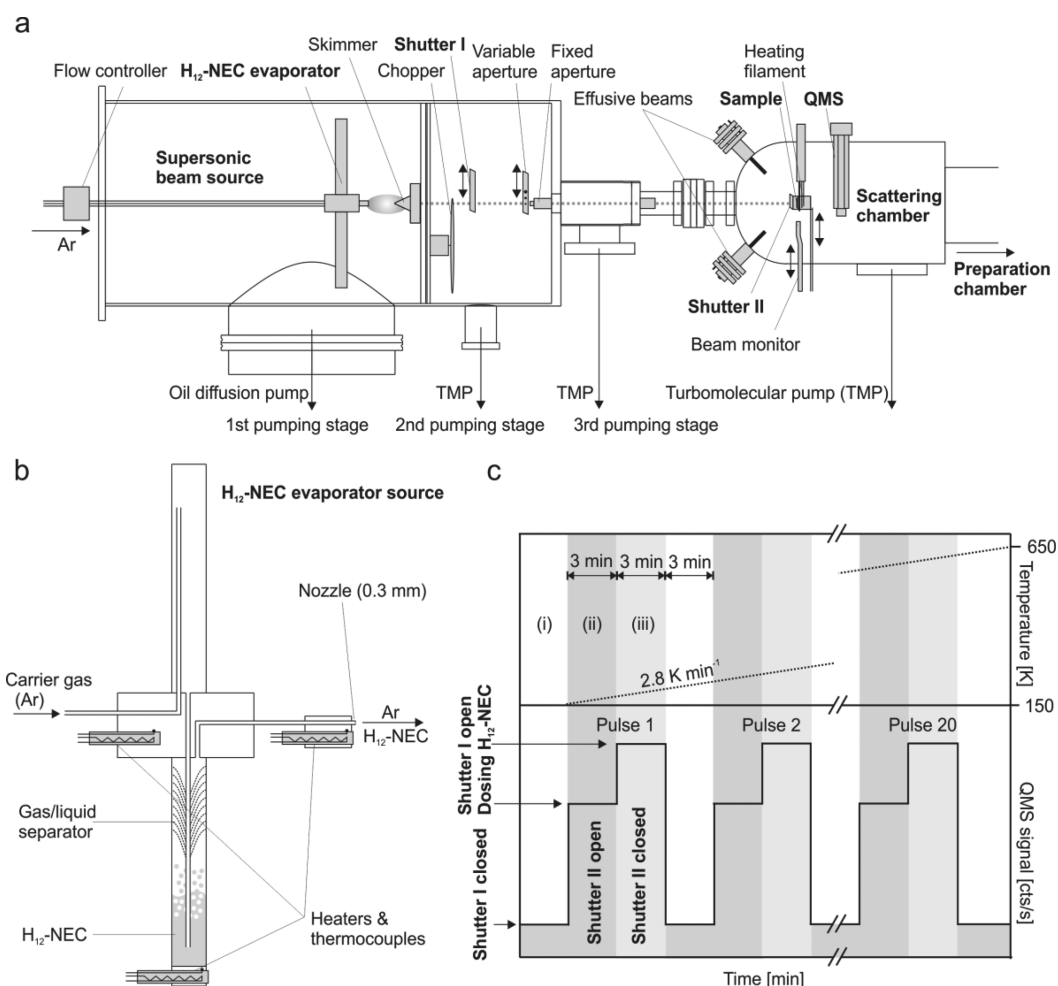
Figure 4. (a) Experimental setup used for the IRAS and MB measurements described in this work (see text for details). (b) MB source used for H_{12}-NEC dosing. (c) Experimental procedure applied in the MB/QMS gas phase analysis experiments with alternating off-time (i), reaction data acquisition (ii), and reference interval (iii) (see the Experimental Section for details).

leaving only the peak at 399.6 eV. No further changes can be seen up to 390 K. Note that, depending on coverage, hydrogen desorbs from Pt(111) just below 300 K,[32] which we believe to be connected with the onset of further dehydrogenation at this temperature. This is in good agreement with our IRAS results, where the band at 1542 cm^{-1} exhibits a strong increase at 323 K. In the C 1s region, dehydrogenation is reflected by the increase in the signal at 284.1 eV and a shift to 284.4 eV, as indicated in Figure 2d. Simultaneously, the peak at 285.2 eV steeply decreases between 280 and 340 K before it vanishes completely at around 380 K. This indicates a further dehydrogenation that is visible only in the C 1s core level because only carbon atoms other than those of the pyrrole ring are affected. We can conclude that complete unloading of the molecule occurs up to around 380 K, first by dehydrogenation around the α-carbon atoms of the pyrrole ring to H_8-NEC, followed by the stepwise dehydrogenation of the two outer rings to NEC, resulting in the complete loss of CH_2 subunits.

When the temperature exceeds 390 K, a new N 1s peak appears at 398.1 eV, while the intensity of the peak at 399.6 eV decreases. Following our previous work, this peak is assigned to carbazole, an undesired side product formed by dealkylation.[31] This reaction occurs directly at the nitrogen atom. In the C 1s region, no comparably strong peak shift can be discerned because of a broadening of the signal arising from the

coexistence of many surface species. At higher temperatures, new signals appear in both the N 1s and C 1s core levels that indicate further decomposition due to loss of hydrogen, C−C bond scission, or both. In contrast with our previous study,[23] the total intensities of both the N 1s and C 1s peaks rise in that temperature range because of the continuous dosing. Obviously, the decomposition products allow for denser packing on the surface.

Gas Phase Analysis via TPMB Experiments. We performed temperature-programmed reaction (TPR) experiments using quadrupole mass spectrometry (QMS) to trace the formation of dehydrogenation and decomposition products in the gas phase. H_{12}-NEC was dosed onto the surface using a supersonic molecular beam (MB) setup. During deposition, the sample was heated from 150 to 650 K at a heating rate of 2.8 K min^{-1}. While heating, we exposed the surface to a total of 20 pulses of H_{12}-NEC. Details on the experimental procedure are described in the Experimental Section and in Figure 4. The QMS raw data are shown in Figure 5a. We chose the following m/z ratios for analysis: 207 amu (H_{12}-NEC), 205 amu (H_{10}-NEC), 203 amu (H_8-NEC), 199 amu (H_4-NEC), and 195 amu (NEC). To obtain additional information on the desorption of potential decomposition products, we also recorded the above-mentioned molecules without ethyl chain, that is, their carbazole analogues: 179 amu (H_{12}-carbazole), 177 amu
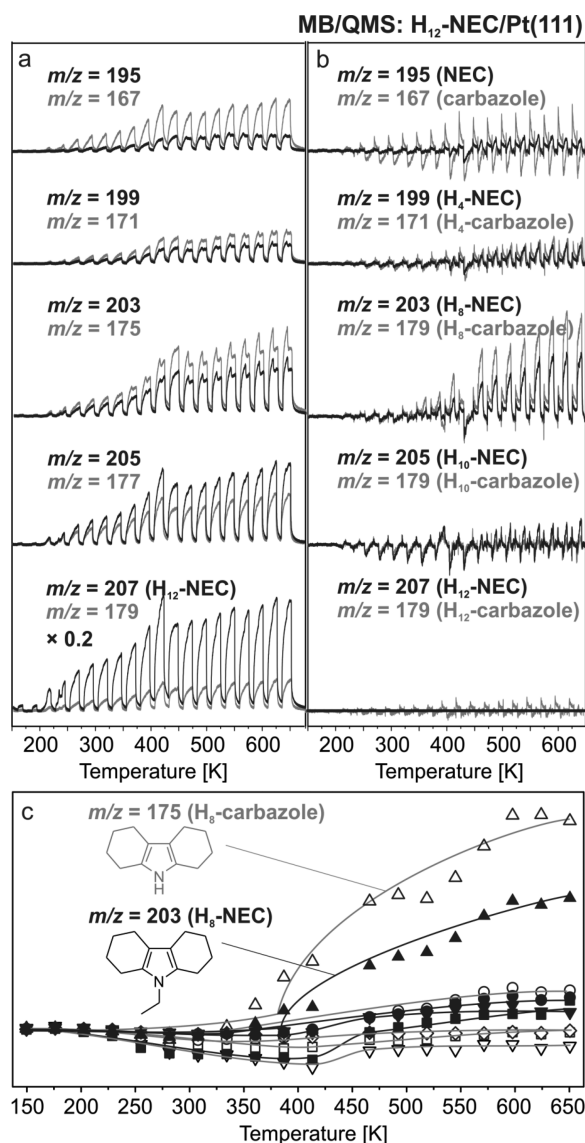
Figure 5. (a) QMS raw data acquired during the temperature-programmed MB/QMS experiment (see Figure 4 and the Experimental Section for details). The m/z values are attributed to the $[M^+]$ signals of the following compounds (including fragmentation peaks): H_{12}-NEC ($m/z = 207$), H_{12}-carbazole ($m/z = 179$, ◇), H_{10}-NEC ($m/z = 205$, ■), H_{10}-carbazole ($m/z = 177$, □), H_8-NEC ($m/z = 203$, ▲), H_8-carbazole ($m/z = 175$, △), H_4-NEC ($m/z = 199$, ●), H_4-carbazole ($m/z = 171$, ○), NEC ($m/z = 195$, ▼), and carbazole ($m/z = 167$, ▽). (b) Gas-phase product traces after subtraction of the fragmentation pattern (see text for details). (c) Integrated gas-phase product peaks as a function of the dosing temperature for each H_{12}-NEC pulse. The 12th pulse was excluded due to an operation error.

(H_{10}-carbazole), 175 amu (H_8-carbazole), 171 amu (H_4-carbazole), and 167 amu (carbazole). The obtained signals are displayed in Figure 5a (NEC derivatives in black, carbazole derivatives in gray). Note that all signals (except the m/z signal at 207 amu) contain contributions from ionization-induced fragmentation of the larger molecules in the mass spectrometer.

From the 207-amu signal, we conclude that almost no desorption H_{12}-NEC occurs up to ∼210 K (corresponding to pulses 1 and 2), indicating a sticking coefficient near unity at low temperatures. This is in agreement with the IRAS data, for

which multilayer formation was observed to vanish between 173 and 223 K.

Above 210 K, desorption is indicated by the continuous increase in the signal at 207 amu. In our previous experiments on Pd(111), we observed a strong desorption peak with a maximum at 210 K, arising from desorption of an accumulated multilayer.[18]

Because of the adsorption/desorption of H_{12}-NEC and its products at the chamber walls, the effective pumping is reduced. This is reflected in the shape of the gas pulses, which are not rectangular but show an exponential tailing (see also our previous work with H_{12}-NEC on Pd(111)[18]). The variation in pulse heights in the 207 amu signal is ascribed to variations in the H_{12}-NEC beam intensity. These are caused by changes in the MB source temperature and the decreasing filling level in the H_{12}-NEC reservoir and are inevitable during a 3-h-long experiment. By normalization to the H_{12}-NEC signal, we compensate for these variations in the other m/z signals. Note that this procedure does not affect the following discussion.

To identify reaction products, we analyze the QMS signals for possible dehydrogenation products with and without dealkylation. With the new pulsing procedure described in the Experimental Section, we are now able to determine the precise cracking pattern and flux of the reactant at each pulse. This information is used to remove the H_{12}-NEC contribution (due to its cracking pattern) from the raw data of all mass signals. The resulting data (Figure 5b) represent the desorbing dehydrogenation and decomposition products only. Figure 5c depicts the integrated intensities of these products per pulse as a function of temperature.

The results indicate that H_{12}-carbazole (179 amu), H_{10}-NEC (205 amu), and H_{10}-carbazole (177 amu) are below the detection limit over the entire temperature range. The small residual signals are due to inaccuracies of the data treatment procedure described above; however, we clearly identify H_8-NEC (203 amu) and its dealkylated counterpart H_8-carbazole (175 amu) as the two main reaction products in the gas phase. As can be seen in Figure 5c, both fragments begin to desorb at ∼390 K. Interestingly, the 175 amu signal exceeds the 203 amu signal from the onset of desorption to the end of the experiment. With increasing temperature, the formation rate for both H_8-NEC and H_8-carbazole increases before it levels off at 600 K. Disregarding the differences in ionization probability, we estimate the average reaction probabilities to H_8-NEC and H_8-carbazole (relative to incoming H_{12}-NEC flux) to 2.8% and 4.4%, respectively (temperature range 390−650 K). It is important to mention that ionization-induced fragmentation of H_8-NEC (203 amu) in the mass spectrometer also contributes to the H_8-carbazole signal (175 amu). Comparison with H_{12}-NEC and NEC[33] suggests, however, that this contribution is minor. Therefore, we conclude that, indeed, H_8-NEC and H_8-carbazole are the main products desorbing from the surface. Note furthermore that C−N bond scission is also observed on real catalysts, but with much lower probability. We attribute this difference to the presence of coadsorbates and molecular fragments on the surface under ambient reaction conditions; this effect will be the focus of future studies.

As discussed before, we identified H_8-NEC as the first stable reaction intermediate in IRAS. The onset for H_8-NEC formation occurred around 223 K, in agreement with our XPS data, where H_8-NEC is identified at 250 K in both the N 1s and C 1s regions. The surface coverage of H_8-NEC increases

with temperature. Release into the gas phase at 390 K is reflected by a decrease in the corresponding signal in XPS.

At this point, we cannot clearly identify any further dehydrogenation or decomposition products in the gas phase, such as H_4-NEC/H_4-carbazole and NEC/carbazole, yet the slight increase in the corresponding signals as a function of temperature suggests that these products are formed with substantially lower reaction probability (note that on a real catalyst, intermediates will readsorb and be further dehydrogenated, whereas under UHV conditions, this is not possible). Our HRXPS experiments revealed, however, that up to 390 K, more strongly dehydrogenated products, such as H_4-NEC and NEC, are formed on the surface. The same observation has been made previously in HRXPS experiments using a different experimental procedure.[23] It is likely that transformations occurring during these dehydrogenation steps are coupled to major changes in the bonding geometry of the molecules to the surface.[20,34,35] Such changes in molecular orientation may give rise to the binding energy shift observed in XPS and to the decreasing IRAS intensity when heating to 473 K. It is noteworthy that H_8-NEC/H_8-carbazole are the dominating dehydrogenation product in the gas phase. These species are formed in the presence of stronger dehydrogenated species present on the surface. The low intensity of H_4-NEC and NEC and their dealkylated counterparts in TPMB, despite the fact that these species are formed, may be explained by their strong interaction with the surface. As a result of π-bonding, these species will prefer a flat-lying orientation and enhanced bonding to the surface.[29,34,35] Thus, adsorption of H_8-NEC is expected to require less space on the surface than stronger dehydrogenated species (H_n-NEC, $n < 8$). As a result of this ensemble effect, the dehydrogenation rate to H_4-NEC and NEC is expected to decrease on a surface partly covered with dehydrogenation intermediates. Thus, the selectivity is shifted to H_8-NEC, which then partly decomposes to H_8-carbazole and desorbs.

Because the temperature threshold for H_8-NEC and H_8-carbazole desorption marks the start of decomposition via C–N bond scission, we speculate that dealkylation may be facilitated by H_8-NEC desorption (as the products of dealkylation will require additional adsorption sites). Below 390 K, abstraction of the ethyl side chain might be suppressed by accumulated dehydrogenation intermediates, which partly cover the surface and thereby limit the number of potential reaction sites. Alternatively, the temperature of 390 K might simply reflect the temperature required for dealkylation on Pt(111).

■ CONCLUSION

We investigated the adsorption and reaction of H_{12}-NEC on Pt(111) under UHV conditions by IRAS, MB methods, and synchrotron radiation-based HRXPS.

Molecular adsorption of H_{12}-NEC occurs up to temperatures between 173 and 223 K without any indication for reaction and with a sticking coefficient near unity. Desorption of the physisorbed multilayer takes place below 223 K.

C–H bond activation at the α-carbon atoms was identified as the initial step of dehydrogenation, starting at ∼223 K. We identified H_8-NEC as the first stable surface intermediate. Upon heating, the H_{12}-NEC monolayer gradually dehydrogenates to H_8-NEC, with a conversion of 40% as soon as the H_{12}-NEC multilayer is desorbed. The reaction drastically accelerates at

300 K, which is associated with an increasing number of free surface sites due to hydrogen desorption at this temperature.

At temperatures up to 380 K, transformation of the CH_2 units to CH within the six-membered rings indicates stepwise dehydrogenation to the final product NEC. The reaction involves a change in adsorption geometry to a flat-lying orientation.

Above 390 K, dehydrogenation of H_{12}-NEC competes with dealkylation, that is, abstraction of the ethyl side chain via C–N bond scission. Dealkylation may be triggered by a decreasing surface coverage at the onset of desorption. Above 420 K, further C–C bond cleavage leads to formation of smaller molecular fragments and atomic species.

A new TPMB procedure permits identification of desorbing products in the gas phase. We identify H_8-carbazole and H_8-NEC as the main species desorbing from the surface. Desorption starts at 390 K and reaches a maximum at ∼600 K. Partial blocking of adsorption sites by strongly bound intermediates is responsible for a shift in selectivity from strong dehydrogenation (e.g., to H_4-NEC and NEC) on the clean surface to partial dehydrogenation to H_8-NEC on the precovered catalyst. As a result, only minor amounts of H_4-NEC or NEC desorb up to 650 K.

A comparison with our previous studies on the reaction of H_{12}-NEC on Pd(111) reveals that the reaction mechanism is very similar. However, the onset of C–N bond scission is shifted to substantially higher temperature on Pt(111) (390 K, i.e., ∼60 K higher as compared with Pd(111)). The temperature threshold for desorption of H_8-NEC shows a concomitant shift. These differences are associated with the different interaction and adsorption energies of the primary intermediate H_8-NEC on Pt(111) and on Pd(111).

■ EXPERIMENTAL SECTION

UHV IRAS and MB Setup. IRAS and TPMB measurements were performed in a UHV system described elsewhere (base pressure below 2×10^{-10} mbar).[36] For both experiments, H_{12}-NEC was deposited via a molecular beam (MB) setup, which is schematically shown in Figure 4a. By applying this technique, a collision-free environment is established, that is, any contact of H_{12}-NEC with the chamber walls prior to interaction with the catalyst surface is avoided. For further details on this technique and its application in model catalysis, see, for example, refs 37–40. The MB source, which is connected to the UHV system, consists of three differentially pumped stages. The expansion chamber is pumped by an oil diffusion pump (pumping speed ∼3000 L s^{-1}), and the second and third stages are pumped with turbomolecular pumps (500 and 60 L s^{-1}, respectively). The MB source features a variable beam-defining aperture. The beam diameter was chosen to slightly exceed the dimensions of the sample (9×11 mm). The beam was aligned, and its intensity was calibrated using a beam monitor, consisting of a movable stainless steel tube with an aperture of 1 mm diameter. The stagnation pressure inside the tube was measured using a highly stable ionization gauge (Granville-Phillips Stabil Ion). For an Ar beam at 300 K, effective pressures of up to 5×10^{-6} mbar are obtained at the sample position.

The H_{12}-NEC beam was generated using a high-temperature saturator cell located inside the expansion chamber (see Figure 4b). Ar (Linde, 99.9999%) as a carrier gas was bubbled through a reservoir of H_{12}-NEC, kept at around 100 °C. The fraction of H_{12}-NEC vapor in the carrier gas was controlled by the

temperature of the H_{12}-NEC reservoir. Ar was used to avoid strong seeding effects, that is, the generation of H_{12}-NEC with high kinetic energies in the supersonic expansion. The Ar/H_{12}-NEC mixture was expanded through a 0.3 mm nozzle into the expansion chamber. All parts of the nozzle setup were individually heated to temperatures slightly above the reservoir temperature to avoid unintended condensation of H_{12}-NEC. The molar fraction of H_{12}-NEC vapor in the carrier gas was then controlled by the temperature of the H_{12}-NEC reservoir. By comparison of the IR spectra at low sample temperature with those obtained with the PVD doser, which is also equipped to the UHV chamber described above, we obtain an estimated H_{12}-NEC flux from the MB source of ~1−3 monolayer/min.[18]

For preparation of the model system for the IRAS and QMS experiments, a Pt(111) single crystal (MaTecK GmbH) was cleaned by several cycles of Ar$^+$ sputtering (E = 1.5 keV, 8 × 10^{-5} mbar Ar, 300 K) annealing (1200 K) and oxidation (5 × 10^{-7} mbar O$_2$, 700 K) in vacuum. The quality of the Pt(111) single crystal was controlled by low energy electron diffraction (LEED). In addition, prior to H_{12}-NEC adsorption, IRAS experiments were conducted to monitor the cleanliness of the surface by CO adsorption experiments at 100 and 300 K.

IRAS Experiments. All IRAS experiments were performed with a vacuum FTIR spectrometer (Bruker IFS 66/v) coupled to the UHV system. During deposition, IR spectra were continuously acquired in a time-resolved fashion with a spectral resolution of 2 cm^{-1}. The acquisition time per spectrum was 60 s.

QMS Experiments. The reaction products formed during our temperature-programmed QMS/MB experiments were identified using a non-line-of-sight quadrupole mass spectrometer in single ion counting mode (Hiden HAL511/PIC), which is connected to the UHV system. In previous experiments, we found that the cracking pattern of H_{12}-NEC, which superimposes the QMS signals of true surface reactions, does not remain constant on the time scale of the experiment. This may be explained by unsteady environmental and instrumental conditions (e.g., accumulation of H_{12}-NEC on the chamber walls). For this reason, we developed a dosing procedure that enables us to trace and subtract the fluctuating fragmentation behavior. The experimental procedure applied is depicted in Figure 4c. The sample was heated from 150 to 650 K at a constant heating rate of 2.8 K min^{-1}. During the temperature ramp, the sample was exposed to 20 H_{12}-NEC pulses, each with a duration of 3 min (ii). The pulsing was performed with an automatic shutter in the second differential pumping stage (shutter I) and a shutter situated directly in front of the sample (shutter II). The sample is exposed to H_{12}-NEC when both shutters are open. Accordingly, the QMS data recorded within this interval contains the "real" signals of all reactants and products. For detecting the contributions arising from ionization-induced fragmentation within the QMS, each pulse was followed by an off time of 2 × 3 min. During the first 3 min (iii), we interrupted the H_{12}-NEC beam with shutter II. The latter ensures that no adsorption (and no reaction) on the sample takes place, while H_{12}-NEC is dosed into the UHV chamber. As a consequence, from this "reference" signal, we can calculate the fraction of QMS-induced cracking of each pulse. These signals are then subtracted from the raw data. After closing both shutters for 3 min (i), the next pulse was performed. In this manner, we are able to differentiate varying background signals and true surface reactions.

UHV XPS Experiments. The XPS measurements were carried out at beamline U 49/2 PGM 1 at the third generation synchrotron BESSY II of Helmholtz-Zentrum Berlin using a transportable UHV setup.[41] In addition to typical surface science tools such as a sputter gun and LEED, a supersonic molecular beam is attached. The sample can be cooled to 120 K using liquid nitrogen and heated to 1400 K using direct heating. For the TPXPS experiments, an additional filament is situated in the back of the crystal to allow for careful heating. This way, we can continuously obtain unperturbed XP spectra for both the adsorption and heating experiments. The time per spectrum was typically on the order of 10 s per spectrum. Moreover, for this particular study, a dosing unit dedicated to the adsorption of H_{12}-NEC and NEC was attached directly to the main chamber. The coverage calibration, as used in the quantitative analysis (Figure 3), was carried out using the known carbon surface coverage of the c(4 × 2) CO superstructure on Pt(111).[42] The fitting procedure included the subtraction of the background and the usage of Doniach−Sunjic functions[43] convoluted with a Gaussian for peak fitting. In the N 1s region, one fit function was used, whereas in the C 1s region, line shapes were used for each species, consisting of two such functions. Because of adsorption from residual gas, there is also a low amount (<0.1 ML) of CO adsorbed on the surface, which was fitted by one function. This approach is similar to the one used in our previous study,[23] described in detail in the respective Supporting Information. The XP spectra were taken using an excitation energy of 380 eV (C 1s) and 500 eV (N 1s), and the resolution was 150 meV (C 1s) and 220 meV (N 1s).

Synthesis of H_{12}-NEC. H_{12}-NEC was synthesized by heating 220 g of NEC (>97%; CAS: 86-28-2, Clariant) in a 600-mL steel autoclave equipped with a gas entrainer stirrer until liquefaction at 85 °C. Subsequently, 10 g of Ru on Al$_2$O$_3$ (5% on support) (Alfa Aesar), 5 g of Pd on Al$_2$O$_3$ (5% on support) (Johnson Matthey), and 4 g MgO (Clariant) were added. The autoclave was closed and purged five times with nitrogen (Linde, 99.999%). The autoclave was then heated to the reaction temperature of 150 °C. Hydrogen (Linde, 99.999%) was introduced at a constant pressure of 65 bar. The stirrer was set to 1200 rpm, and the reaction was started. After 72 h of reaction, the autoclave was cooled to room temperature, the product removed from the autoclave, and the catalyst was filtered. Product distillation yielded H_{12}-NEC with a purity above 99% in a mixture of three conformers.

■ ASSOCIATED CONTENT

Ⓢ Supporting Information
Complete series of the time-resolved IRAS spectra at 100, 123, 173, 223, 273, 323, 373, 423, and 473 K. The measurement time per spectrum was 1 min, the total exposure time was 30 min. This information is available free of charge via the Internet at http://pubs.acs.org.

■ AUTHOR INFORMATION

Corresponding Author
*Fax: (+49)9131-858867. E-mail: joerg.libuda@fau.de.
Notes
The authors declare no competing financial interest.

■ ACKNOWLEDGMENTS

■ REFERENCES

(1) Eberle, U.; Felderhoff, M.; Schüth, F. *Angew. Chem.* **2009**, *121*, 6732.

(2) von Wild, J.; Friedrich, T.; Cooper, A.; Tosel, B.; Muraro, G.; Tegrotenhuis, W.; Wang, Y.; Humble, P.; Karim, A.; Stolten, D.; Grube, T. *Energy Environm.* **2010**, *78−4*, 188−197.

(3) Ghosh, T. K.; Prelas, M. A. *Energy Resources and Systems*; Springer Science+Business Media B. V.: New York, 2011; Vol. 2: Renewable Resources, Band 2.

(4) Tzimas, E.; Filiou, C.; Peteves, S. D.; Petten, J. B. V., *Hydrogen Storage: State-of-the-Art and Future Perspective*; European Commission, Institute for Energy: Petten, NL, 2003.

(5) James, B. D. *Prepr. Symp., Div. Fuel Chem., Am. Chem. Soc.* **2008**, 568−569.

(6) Teichmann, D.; Arlt, W.; Wasserscheid, P. *Int. J. Hydrogen Energy* **2012**, *37*, 18118.

(7) Teichmann, D.; Arlt, W.; Wasserscheid, P.; Freymann, R. *Energy Environ. Sci.* **2011**, *4*, 2767−2773.

(8) Teichmann, D.; Stark, K.; Müller, K.; Zöttl, G.; Wasserscheid, P.; Arlt, W. *Energy Environ. Sci.* **2012**, *5*, 9044.

(9) Pez, G. P.; Scott, A. R.; Cooper, A. C.; Cheng, H.; Bagzis, L. D.; Appleby, J. B. International Patent WO/2005/000457, 2005.

(10) Crabtree, R. H. *Energy Environ. Sci.* **2008**, *1*, 134−138.

(11) Eblagon, K. M.; Tam, K.; Yu, K. M. K.; Tsang, S. C. E. *J. Phys. Chem. C* **2012**, *116*, 7421−7429.

(12) Zhao, H. Y.; Oyama, S. T.; Naeemi, E. D. *Catal. Today* **2010**, *149*, 172−184.

(13) Scherer, G. W. H.; Newson, E. *Int. J. Hydrogen Storage* **1998**, *23*, 19−25.

(14) Eblagon, K. M.; Rentsch, D.; Friedrichs, O.; Remhof, A.; Zuettel, A.; Ramirez-Cuesta, A. J.; Tsang, S. C. *Int. J. Hydrogen Energy* **2010**, *35*, 11609−11621.

(15) Libuda, J.; Freund, H.-J. *Surf. Sci. Rep.* **2005**, *57*, 157−298.

(16) Chen, M. S.; Goodman, D. W. *Catal. Today* **2006**, *111*, 22−33.

(17) Freund, H.-J. *Chem.—Eur. J.* **2010**, *16*, 9384−9397.

(18) Amende, M.; Schernich, S.; Sobota, M.; Nikiforidis, I.; Hieringer, W.; Assenbaum, D.; Gleichweit, C.; Drescher, H.-J.; Papp, C.; Steinrück, H.-P.; Görling, A.; Wasserscheid, P.; Laurin, M.; Libuda, J. *Chem.—Eur. J.* **2013**, *19*, 10854−10865.

(19) Sobota, M.; Nikiforidis, I.; Amende, M.; Zanón, B. S.; Staudt, T.; Höfert, O.; Lykhach, Y.; Hieringer, W.; Laurin, M.; Assenbaum, D.; Wasserscheid, P.; Steinrück, H.-P.; Görling, A.; Libuda, J. *Chem.—Eur. J.* **2011**, *17*, 11542−11552.

(20) Sotoodeh, F.; Smith, K. J. *J. Phys. Chem.* **2012**, *117*, 194−204.

(21) Papp, C. In-situ investigations of adsorbed hydrocarbons −model systems of heterogeneous catalysis. Ph.D. thesis, FAU Erlangen-Nürnberg, 2007.

(22) Ihm, H.; White, J. M. *J. Phys. Chem. B* **2000**, *104*, 6202−6211.

(23) Gleichweit, C.; Amende, M.; Schernich, S.; Zhao, W.; Lorenz, M. P. A.; Höfert, O.; Brückner, N.; Wasserscheid, P.; Libuda, J.; Steinrück, H.-P.; Papp, C. *ChemSusChem* **2013**, *6*, 974−977.

(24) Hoffmann, F. M. *Surf. Sci. Rep.* **1983**, *3*, 107.

(25) Pearce, H. A.; Sheppard, N. *Surf. Sci.* **1976**, *59*, 205−217.

(26) Baddeley, C. J.; Hardacre, C.; Ormerod, R. M.; Lambert, R. M. *Surf. Sci.* **1996**, *369*, 1−8.

(27) Stuve, E. M.; Madix, R. J. *J. Phys. Chem.* **1985**, *89*, 3183−3185.

(28) Sexton, B. A. *Surf. Sci.* **1985**, *163*, 99−113.

(29) Saeys, M.; Reyniers, M.-F.; Neurock, M.; Marin, G. B. *Surf. Sci.* **2006**, *600*, 3121.

(30) Stacchiola, D.; Azad, S.; Burkholder, L.; Tysoe, W. T. *J. Phys. Chem. B* **2001**, *105*, 11233.

(31) Morin, C.; Simon, D.; Sautet, P. *Surf. Sci.* **2006**, *600*, 1339.

(32) Poelsema, B.; Lenz, K.; Comsa, G. *J. Phys.: Condens. Matter* **2010**, *22*.

(33) National Institute of Standards and Technology, *Chemistry WebBook*, http://webbook.nist.gov/; accessed 17.09.2013.

(34) Crawford, P.; Burch, R.; Hardacre, C.; Hindle, K. T.; Hu, P.; Kalirai, B.; Rooney, D. W. *J. Phys. Chem. C* **2007**, *111*, 6434−6439.

(35) Crawford, P.; Burch, R.; Hardacre, C.; Hindle, K. T.; Hu, P.; Rooney, D. W. *J. Chem. Phys.* **2008**, *128*, 105104.

(36) Desikusumastuti, A.; Staudt, T.; Happel, M.; Laurin, M.; Libuda, J. *J. Catal.* **2008**, *260*, 315.

(37) Libuda, J. *Chem. Phys. Chem.* **2004**, *5*, 625−631.

(38) Libuda, J.; Meusel, I.; Hartmann, J.; Freund, H.-J. *Rev. Sci. Instrum.* **2000**, *71*, 4395.

(39) Valleau, J. P.; Deckers, J. M. *Can. J. Chem.* **1965**, *43*, 6−17.

(40) Kleyn, A. W. *Chem. Soc.* **2003**, *32*, 87.

(41) Denecke, R.; Kinne, M.; Whelan, C. M.; Steinrück, H.-P. *Surf. Rev. Lett.* **2002**, *9*, 797.

(42) McEwen, J. S.; Payne, S. H.; Kreuzer, H. J.; Kinne, M.; Denecke, R.; Steinrück, H. P. *Surf. Sci.* **2003**, *545*, 47−69.

(43) Doniach, S.; Sunjic, M. *J. Phys. C: Solid State Phys.* **1970**, *3*, 285.